CrossMark

The overall effect of reactive rubber nanoparticles and nano clay on the mechanical properties of epoxy resin

Mona A. Ahmed [a,*]**, Usama F. Kandil** [a]**, Neviene O. Shaker** [a]**, Ahmed I. Hashem** [b]

[a] Polymer Nanocomposites Center, Egyptian Petroleum Research Institute, Nasr City 11727, Cairo, Egypt
[b] Department of Chemistry, Faculty of Science, Ain Shams University, Cairo, Egypt

ARTICLE INFO

ABSTRACT

Epoxy resin, a thermoset polymer matrix used for technical applications; exhibit some outstanding properties such as high modulus, high chemical resistance and high dimension stability. However, the high crosslink density of epoxy makes this material brittle with low impact strength and poor resistance to crack propagation, which limits their many end use applications. It is an important objective to explore new routes toward toughening of epoxy resins without affecting stiffness, strength, and glass temperature. The main objective of this work is to incorporate reactive rubber nanoparticles (RRNP) and organically modified nanoclay (Cloisite-30B) into epoxy matrix with the aim of obtaining improved material with higher toughness without compromising the other desired mechanical properties. Epoxy hybrids nanocomposites containing RRNP, Cloisite-30B and RRNP/Cloisite-30B mixture were synthesized and characterized to compare the different properties which normally result from the use of single filler and hence aiming to improve toughness/stiffness balance.

1. Introduction

Epoxy polymers are widely used for the matrices of fibre-reinforced composite materials and as adhesives. When cured, epoxy polymers are amorphous and highly-crosslinked (i.e. thermosetting) polymers. This microstructure results in many useful properties for structural engineering applications, such as a high modulus and failure e strength, low creep, and good performance at elevated temperatures. However, the structure of such epoxy polymers also leads to a highly undesirable property in that they are relatively brittle materials, with a poor resistance to crack initiation and growth.

So, toughening of brittle epoxy thermosets has been intensively studied in the past few decades since the lack of toughness is one of the major reasons limiting their more widespread engineering applications (Hsieh, Kinloch, Masania, & Taylor, 2010).

One of the most successful strategies of improving the fracture toughness of epoxy is to introduce a second phase into the epoxy matrix. In these systems, the fracture

toughness can be increased by forming multiphase morphology with the ability to initiate various toughening mechanisms during crack growth (Bashar, Sundararaj, & Mertiny, 2011).

One of the successful methods used to toughen (EP) epoxy is the incorporation of the rubber phase into the brittle epoxy matrix, which may be achieved by the use of reactive liquid rubber or preformed rubber particles. The compatibility between liquid rubber and resin must be matched carefully in order to achieve phase separation during cure and simultaneously provide adequate interfacial adhesion (Pascault, 1995). The phase-separated rubber particles are presumed to act as stress concentrators initiating energy absorbing "toughening" processes. According to the literature, the most common micromechanical processes responsible for the increase in fracture toughness are localized shear yielding of the epoxy matrix, plastic void growth in the matrix, which is initiated by cavitation or deboning of the rubber particles, and rubber particle bridging behind the crack tip (Yi, Wiedmaier, & Schmauder, 2015).

The early advances of McGarry and the re-searchers at B.F. Goordrich were the compatibility matching that has been achieved by varying molecular architectures and reactive end groups of liquid rubbers, such as butadiene acrylonitrile copolymers containing carboxyl (CTBN), amine (ATBN), or epoxy (ETBN) reactive end groups. Other elastomeric modifiers that have been studied included acrylate elastomers (Ratna & Banthia, 2004) and polysiloxanes. Liquid polyethers like poly(propylene oxide) (Harani, Fallahi, & Bakar, 1998) or poly(-tetrahydrofuran) have also been used as toughening agents. Modification of their end groups in order to tailor phase separation behavior and adhesion to the matrix via chemical bonds have easily been achieved. However, improvement of fracture toughness by the addition of liquid rubber modifiers is frequently associated with softening of the matrix due to matrix flexibilization. This is attributed to the fact that the modulus of the modifier is much lower than the modulus of the matrix.

Nanocomposite technology using organophilic layered silicates as an *in-situ* route to nano-reinforcement offers new opportunities for the modification of thermoset micromechanics. Large improvements of mechanical and physical properties including modulus (Kojima et al., 1993), barrier properties, flammability resistance, and ablation performance have been reported for this type of material at low silicate content. In principle, it should be possible to compensate matrix flexibilization via matrix reinforcement using organophilic layered silicates.

Polymer/layered silicate nanocomposites were first developed by researchers from Toyota based on the thermoplastic polyamide-6 (Sharmin et al., 2011) and have been extended to thermosets by Giannelis and Pinnavaia (Messersmith & Giannelis, 1994). Polymer/layered silicate composites are usually divided into three general types: conventional composites with the silicate acting as a filler on the microscale, intercalated nanocomposites based on the insertion of a polymer in between the silicate layers which remain in a long-range order and exfoliated nanocomposites in which individual silicate layers are dispersed in the polymer matrix. Only few attempts have been made so far to combine liquid rubbers and layered silicates to achieve hybrid nanocomposites. Many patents are dealing with a particulate of inorganic fillers which have been extensively used in combination with liquid rubbers to enhance the mechanical properties of epoxy resins and other polymeric matrices in industry (MÜlhaupt, 1994). Also another family of epoxy hybrid composites is materials containing both glass beads and liquid rubbers (Michael, DiBerardino, & Raymond, 2009).

Therefore, the main objective of this work is to incorporate both reactive rubber nanoparticles (RRNP) and organically modified nanoclay (Cloisite-30B) into epoxy matrix with the aim of obtaining improved material with toughness higher than neat epoxy, epoxy/clay and epoxy/RRNP hybrids without compromising the other desired mechanical properties. Epoxy hybrid nanocomposites containing both fillers; organo-modified montmorillonite (o-mmt) and reactive rubber nanoparticles (RRNP); were synthesized in order to combine their enhancing properties which normally result from the use of the single fillers and hence aiming to improve toughness/stiffness balance. Although the fracture and deformation behavior of the epoxy–nanocomposites have been intensively studied at the macro-level over the past decade, less attention has been paid to the stress transfer mechanism in the nano to micro-level behavior of nanoclay and nanorubber interactions with epoxy.

2. Experimental methods

2.1. Materials

Oleic acid is a fatty acid (Adwic co) as a surfactant, potassium hydroxide (TOK co), toluene (fision, AR), chloroform (Aldrich, 99.8%) are all of analytical grade and were used as received. Deionized water was used for all latices. Divinylbenzene (Merck, inhibited by tert-butyl catechol) as a crosslinker was washed over 10 wt% NaOH solution. Styrene-co-butadiene rubber (SBR-latex) (Sika Co.), benzoyl peroxide (BPO) (moistened with 25% water, Loba Chemie), ammonium persulphate (Morgan, 98%), and HCL (37%, Aldrich CO), methanol (95%, Aldrich CO) were used as received.

In our research investigation, we used SBR-latex; supplied by Sika Company; which has the formulations shown in Table 1. This latex contains anionic and nonionic surfactants; (Sodium dodecyl sulfate, SDS with HLB = 8) and (Polyoxyethylene (100) stearyl ether, Brij 700 with HLB = 19), respectively. The HLB value represents the tendency of an emulsifier (surfactant) to act as an oil-soluble or as a water-soluble type of emulsifier (Becher, 1965). The HLB values for the SBR latex surfactants indicate both oil and water soluble substances,

Table 1 – Chemical composition of commercial SBR-latex (Ohama, 1995).

Material	Parts by weight
Styrene	64.0
Butadiene	35.0
Vinyl carboxylic acid	1.0
Nonionic surfactant	7.0
Anionic surfactant	0.1
Water	105.0

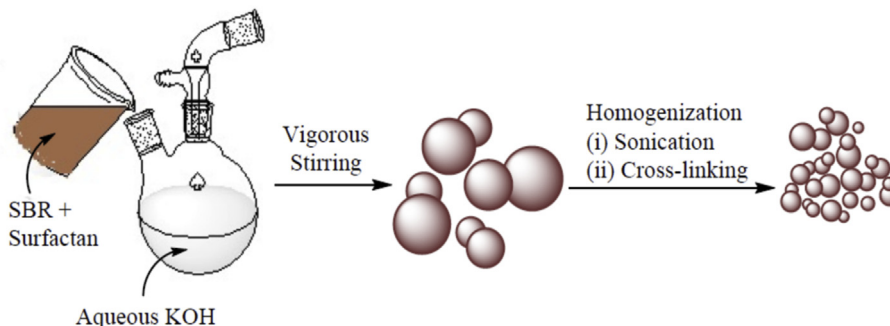thus it is an adequate media for the dispersion of RRNP preparation step.

The resin is a low viscosity 100% reactive diluted liquid based on bisphenol-A containing EPOTUF® 37–058 which is C_{12}–C_{14} glycidyl ether, while the hardener is Aliphatic Amine EPOTUF® 37–614. The viscosity of the resin at 25 °C is 600 cps. The resin to hardener mixing ratio is 2:1, the pot life at 26 °C is 30–45 min, while setting time is 5–6 h hand, and the curing time is 24–28 h at room temperature. This type of epoxy has relatively low viscosity, which facilitates the dispersion of both RRNP and Cloisite30B during the fabrication process. The tensile strength and elongation were reported as 62–69 MPa and 2.2–2.5% respectively. The flexural strength and modulus were reported as 117–131 MPa and 3105–3240 MPa respectively. The clay used to synthesize epoxy–clay nanocomposite is Cloisites30B supplied by Southern Clay Products, Inc. Cloisites30B is an off white color natural montmorillonite modified with a quaternary ammonium salt of density 1.98 g/cm³. X-ray diffraction d-spacing (001) was reported as 18.5 Å.

2.2. Synthesis of styrene-co-butadiene rubber (SBR) nanoparticles by emulsification technique

10.0 g SBR (styrene-co-butadiene rubber) was dissolved in 100 ml toluene containing (5–7) wt% divinylbenzene as a crosslinker. 5 wt% of oleic acid and about 1.0 wt% of benzoyl peroxide as a free radical initiator was added. In a second step, the whole organic phase was slowly added to a vigorously stirred solution of KOH in 500 ml deionized H_2O and about 1.0 wt% of ammonium per sulphate such that the final emulsion has a pH slightly alkaline. After strong stirring for 30 min, the emulsion was homogenized by ultra-sonification for another 60 min in an ultrasonic processor homogenizer operating under nitrogen as shown in Scheme 1. The flask was purged with N_2 for 30 min before rising the temperature to 90 °C. Reaction time was ranged from 2 to 6 h, depending on the viscosity of the samples and consequently on the molecular weight of the used rubber. The product was coagulated by HCl/methanol, re-dispersed in chloroform and precipitated with methanol to remove the surfactant before an overnight drying under vacuum.

2.3. Epoxidation of rubber nanoparticles (Crivello & Song, 2000; Kim, 2001)

Rubber nanoparticles (5.0 g) were dispersed in 80 ml toluene in a flask with 1.8 g of m-chloroperbenzoic acid. The reaction was

performed at 70 °C for 4 h with stirring under N_2 atmosphere, and then the products was obtained by precipitating with methanol, washed and vacuum dried.

2.4. Fabrication of epoxidized rubber nanoparticles/epoxy nanocomposite

The rubber nanoparticles were first dispersed in chloroform before mixing with the epoxy base resin using ultrasonicator. This was followed by evaporation of chloroform and adding the epoxy hardener; then casting in molds for flexural testing. According to ASTM D790-03; five rubber nanoparticle contents were examined including 0, 3, 5, 7 and 10 wt% of resin.

2.5. Fabrication of clay nanoparticles/epoxy nanocomposite

Five nanoclay contents were examined including 2, 4, 6, 8 and 10 wt% of resin. Relatively, high operating temperature and ultrasonication facilitate diffusion of oligomers inside the clay galleries. The nanoclay was dispersed in the epoxy resin at 120 °C using a mechanical stirrer at about 1200 rpm for 2 h followed by further dispersion with an ultrasonic probe for 2 h at 60 °C. While mixing, the beaker was placed in a cold water bath to avoid temperature increase of the dispersion during the sonication process and the temperature was monitored (Kandil, 2005). Then, the dispersion was cooled to room temperature followed by adding the hardener, stirred for about two more minutes. The epoxy–clay nanocomposite was then casted in molds and left to cure at room temperature for 14 days for flexural testing (Fig. 1).

2.6. Characterization

Fourier transform infrared (FTIR) spectra were recorded using Nicolet IS-10 FTIR spectrophotometer–Thermo Fisher Scientific. The specimens were finely grinded and mixed with KBr then these mixtures were compressed into pellet forms. FTIR spectral analysis was performed within the wave number range of 400–4000 cm⁻¹.

All ¹H NMR spectra were recorded at room temperature on a Bruker AM-300 spectrometer with the DISNMR software. The NMR samples were prepared in d-chloroform that is a good solvent for epoxy–Rubber nanocomposite.

X-ray diffraction (XRD) analyses were performed for the epoxy/clay nanocomposites by using XPERT-PRO-Panalytical-Netherland in Nanotechnology characterization Centre (NCC),
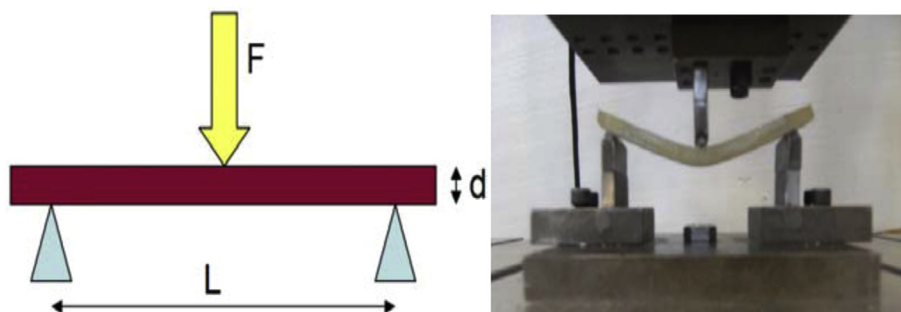

Scheme 1 – Synthesis of rubber nanoparticles.

Fig. 1 – Beam under 3 point bending.

Agriculture of Research Centre (ARC) using CuK, radiation $\lambda = 1.54$ Å and equipped with computerized data collection and analytical tools. The X-ray source was operated at voltage of 45 kV and filament current of 30 mA. All samples were scanned in 2θ from 0.4 to 10° at a rate of 1°/min. The relation between the d-spacing (d) and the angle of diffraction θ was obtained according to Bragg's law (Giannelis, 1996)

$$\lambda = 2d \ \sin \theta \tag{1}$$

where λ is the wavelength used in nm, d is the d-spacing between nano-platelets in nm, and θ is the diffraction angle in degrees.

Bulk morphology in the polymer films was examined by Scanning Electron Microscope (SEM), using a Topcon International Scientific Instruments ISI-SX-40 with secondary electron imaging. SEM samples were prepared from films cryo-fractured in liquid N_2. Samples were mounted on an aluminum stub and gold coated to form a conductive coating.

The morphological features of epoxy nanocomposites were examined by transmission electron microscopy (TEM) where the images were produced using high resolution JEOL-2100F TEM at 200 kV. Measurements were conducted by preparing the samples in a diluted ethanol colloidal mixture which was sonicated for 15 min. A drop of this solution was placed on a carbon-coated Cu TEM grid. After drying, the grid was connected to the microscope and images were captured.

Flexural testing was used to characterize flexural strength and stiffness of epoxy nanocomposites to verify consistency in samples. Flexural modulus was measured using three point bending tests in accordance to ASTM (D790-03). Displacement-controlled test was performed with rate of 0.4 mm/min Fig. 1represents the flexural testing set-up. The flexure stress (σ_f)-strain (ϵ_f) relationships were then obtained according to Eqs. (2) and (3) respectively.

$$\sigma_f = \frac{3PL}{2bd^2} \tag{2}$$

$$\varepsilon_f = \frac{6Dd}{L^2} \tag{3}$$

Where P is the applied load, L is the span length, b is the width of the specimen, d is the depth of the specimen, and D is the deflection of mid-span.

Dynamic mechanical analyzer supplied from Triton Technology (TTDMA), U.K., was used to study the viscoelastic properties of the nanocomposites as a function of clay concentration and then correlated with the morphology. Modulus was evaluated using shear mode according to ASTM standards (ASTM D 4065-01). Ring specimens with diameter of 10 mm were analyzed at room temperature and 1 Hz frequency. The number average molecular weight between crosslinks of neat epoxy, i.e. M_c value, can be calculated from a variety of methods (Lee & Yee, 2000). In this study, Eq. (4), which is based on the theory of rubber elasticity (Ferry, 1980), was applied. Where q is the front factor (assumed as 1 in this work); T is the temperature (K); ρ is the density of the matrix at temperature T; R is the universal gas constant, and G_r is the storage shear modulus in the rubbery region at temperature T.

$$M_C = \frac{q\rho RT}{G_r} \tag{4}$$

3. Results and discussion

3.1. Synthesis of functional rubber nanoparticles

This class of functional rubber nanoparticles is represented by Formula III (see Fig. 2), in which the rubber nanoparticle is a cross-linked styrene-co-butadiene (SBR) rubber with a low glass transition temperature (Tg < −40 °C) and a sub-micron particle size. The reactive double bond moieties located on or near the surface, can easily be transferred to OH, COOH, NH_2, halide, epoxide, anhydride, borane, silane and mixtures, which can engage in chemical reactions with matrix material during the reactive blending, extrusion and polymerization processes. A major advantage of these rubber nanoparticles (III) is the existence of a controlled quantity of pendent double bond moieties that are versatile in many chemical reactions, including cross-linking, functionalization, polymerization, etc.

During the cross-linking reaction to form stable styrene-co-butadiene(SBR) rubber nanoparticles; the internal double bonds units react with each other by the enhancement of the cross linking agent (divinylbenzene DVB) via radical addition reaction. Consequently, most of external double bond units on or near the surfaces are much more difficult to find each other and remained on the surfaces. This result is valuable in the subsequent functionalization reactions.
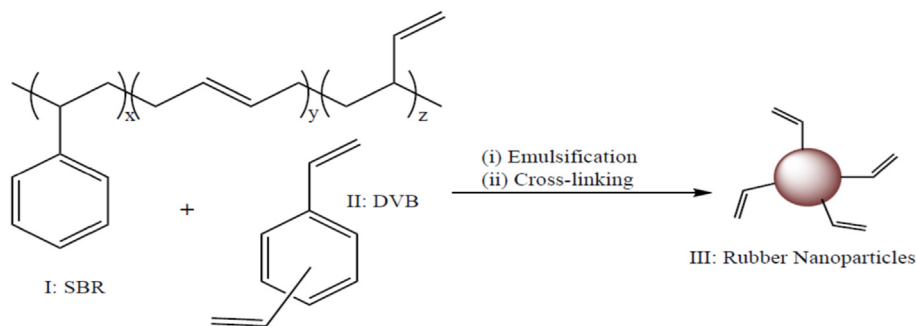
Fig. 2 – Synthesis of functional rubber nanoparticles.

3.2.   Functionalization of rubber nanoparticles

Epoxidizing these nanoparticles produces the rubber core (Reactive Rubber Nanoparticles; RRNP); represented by the formula shown in Fig. 3; that have been mixed with the base material of the epoxy resin before adding the hardener. Therefore, the epoxy base containing these epoxidized-reactive rubber nanoparticles (RRNP) was cured with the curing agent which basically is a diamine. In this case, the hardener; the diamine; reacts with both kinds of the present epoxy groups forming core–shell structure (Fig. 4).

3.3.   Characterization of epoxy nanocomposites

3.3.1. ^{1}H NMR spectroscopy
The epoxidized rubber nanoparticles (RRNP) was character-ized by ^{1}H NMR spectrum where the formation of epoxy groups is assured by the appearance of two new signals cor-responding to the protons of the epoxy group with the reduction in area of the signal of vinyl double bond protons. Fig. 5 shows the ^{1}H NMR spectra of (a) SBR and (b) epoxidized SBR rubber nanoparticles. The ^{1}H NMR spectrum of SBR (Fig. 5a) shows a signal at $\delta = 5.4$ ppm that is attributed to
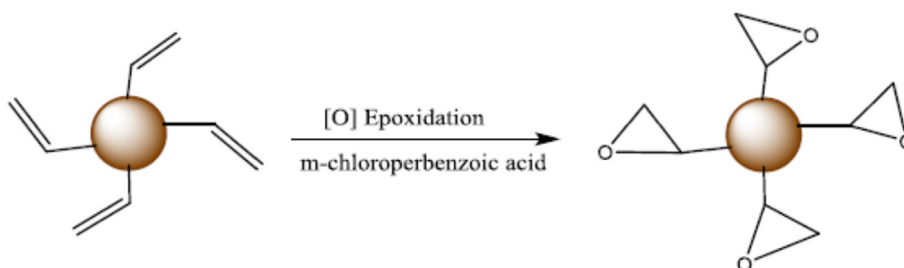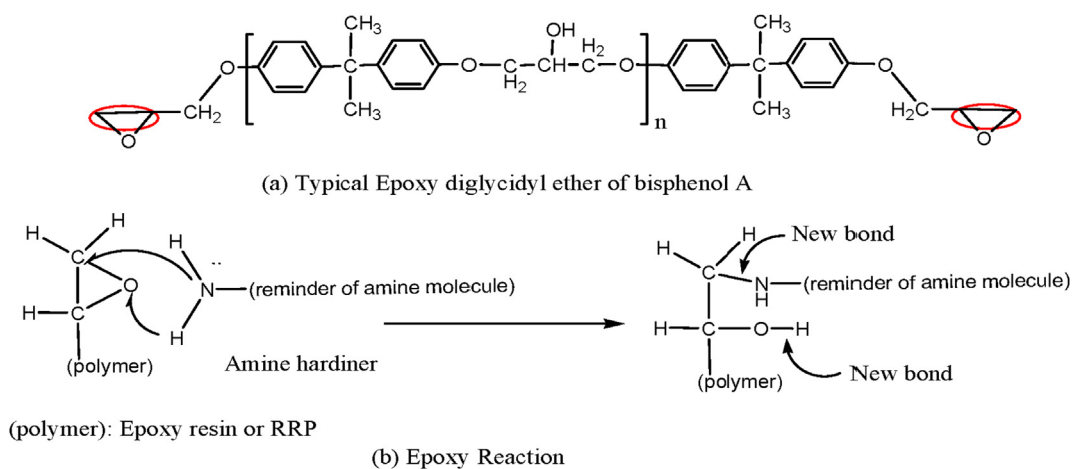

Fig. 3 – Epoxidation of rubber nanoparticles.

(a) Typical Epoxy diglycidyl ether of bisphenol A

(polymer): Epoxy resin or RRP

(b) Epoxy Reaction
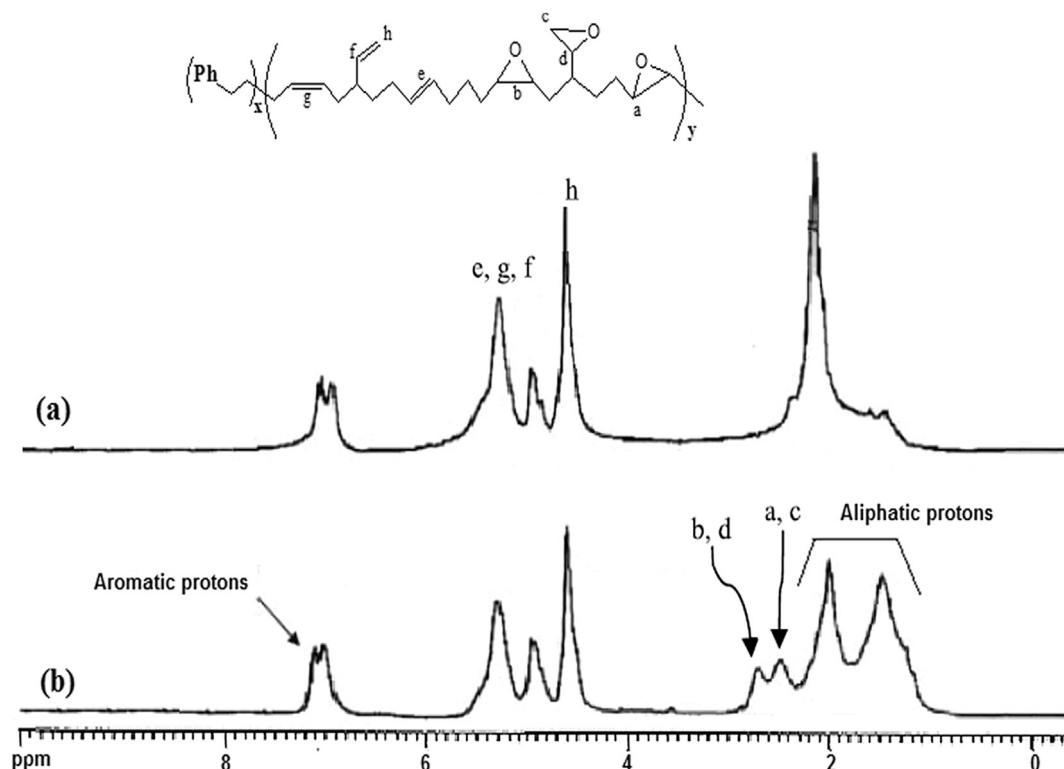
Fig. 4 – (a) Typical epoxy and (b) Epoxy reaction.

Fig. 5 – ¹H NMR (a) SBR, and (b) epoxidized rubber nanoparticles.

trans- and *cis-*1,4 hydrogens and a signal at δ = 4.9 ppm for two terminally vinylic hydrogens. In addition, SBR demonstrates a broad signal at 7.0 ppm, which denotes the five hydrogen atoms of the phenyl ring.

The ¹H NMR spectrum of epoxidized SBR (Fig. 5b) shows two new signals at 2.45 and 2.7 ppm, which can be attributed to the cis- and trans-epoxy groups respectively (Rajabi, Alavi Nikje, & Taslimipour, 2010). By comparing (a) and (b) spectra, it is clear that the appearance of two new signals is attributed to the epoxy ring protons formed via epoxidation reaction with *m*-chloroperbenzoic acid with the reduction in signal area of the vinylic protons.

3.3.2. FTIR spectroscopy

The FT-IR spectra of SBR and epoxidized SBR are shown in Fig. 6a,b, respectively. By comparing both spectra, it is clear that (Fig. 6a) showed a band at 699 cm⁻¹ that is related to 1,4-*cis*, a band at 910 cm⁻¹ to 1,2-vinyl double bonds, and a band at 969 cm⁻¹ to 1,4-*trans*, respectively. In the FT-IR spectrum of epoxidized SBR (Fig. 6b) the bonds of stretching and contracting in phase of all epoxy rings were observed at about 1258 and 842 cm⁻¹(Rajabi et al., 2010).

3.4. RRNP/epoxy nanocomposite

After functionalization, the epoxy groups created on RRNP surface have been chemically connected into the epoxy matrix as represented in Scheme 2. This was assured by the morphological study of the formed nanocomposites using Scanning Electron Microscope (SEM) and Transmission Electron Microscope (TEM).

3.4.1. Scanning electron microscopy (SEM)

The epoxy functional group located on the surface of rubber nanoparticles enhances the reactivity of these particles during the curing reaction of epoxy. This can be observed from Fig. 7 which shows the SEM micrographs of the fracture surface of simple blend between unfunctionalized rubber nanoparticles and epoxy resin (Fig. 7-left) with epoxidized RRNP particles/epoxy reactive blend (Fig. 7-right).

It is clear from these photos that; in a simple blend, there are a lot of concave holes and convex particles in the fracture surface which indicates the weakness of adhesion between the rubber nanoparticles and the epoxy matrix. On the other hand, this view disappeared in the reactive blend between epoxidized nanoparticles with the epoxy matrix. This is attributed to the incorporation of the surface epoxy groups of the particles during the epoxy curing reaction. This reaction enhances the adhesive force between the epoxy matrix and the particles and exceeds the matrix cohesive force.

3.4.2. Transmission electron microscopy (TEM)

The cross-linked rubber nanoparticles are uniformly distributed in the epoxy matrix as shown in the TEM micrograph of the epoxy/RRNP reactive blend (Fig. 8). This is an essential requirement for toughening mechanism. Consequently, the resulting core–shell reactive rubber nanoparticles (RRNP) are homogeneously embedded in the epoxy matrix with chemical interfacial interactions as illustrated by the schematic representation of a toughened epoxy sample (Scheme 2).
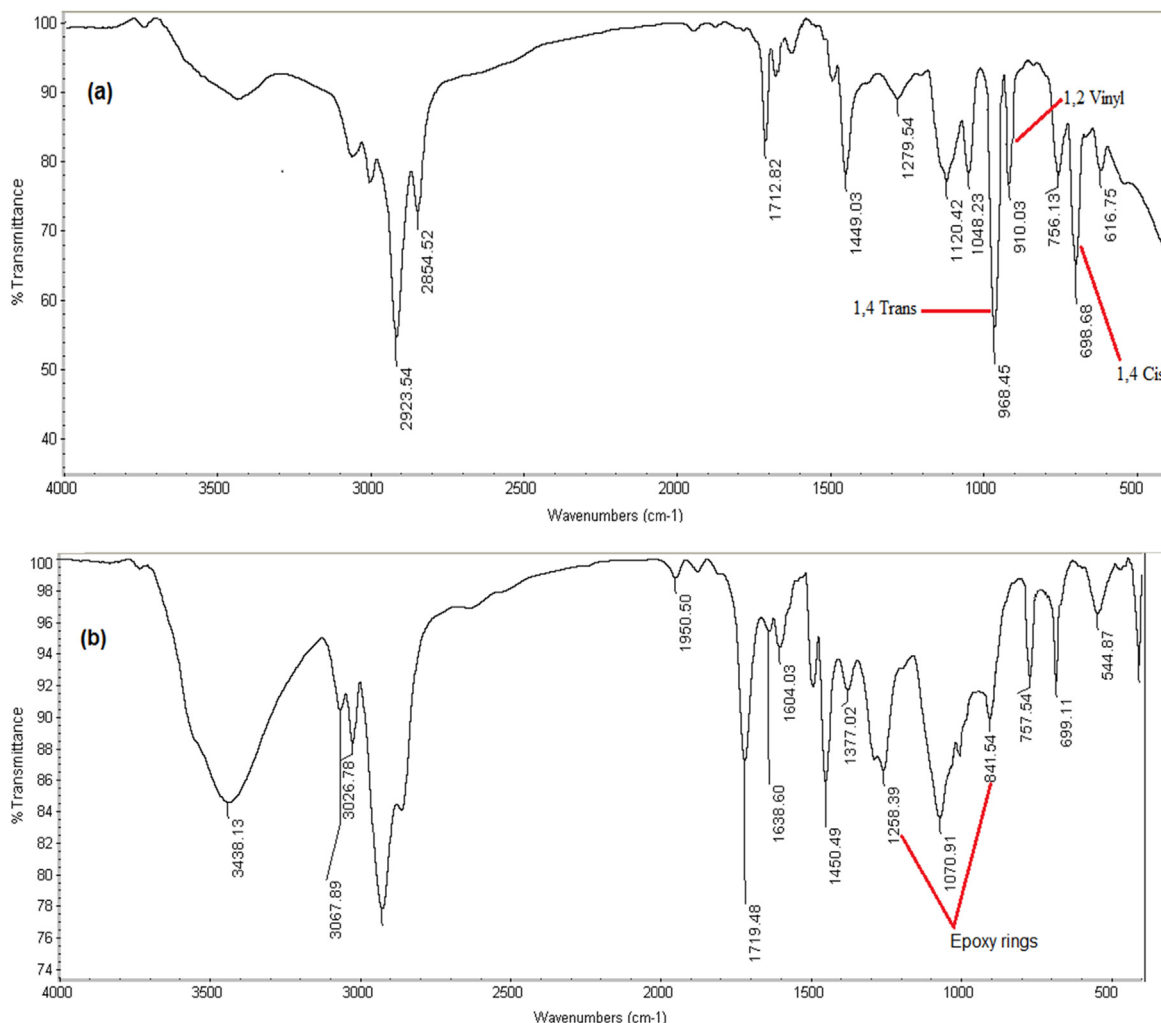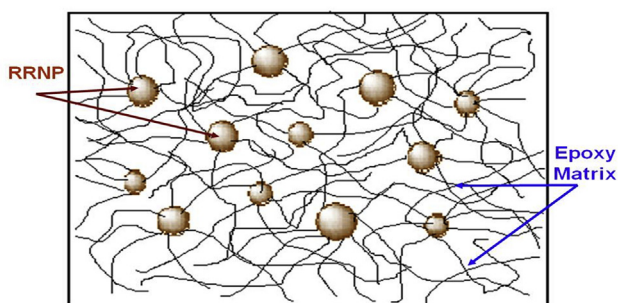
Fig. 6 – a) FTIR of SBR, b) epoxidized SBR nanoparticles.

Scheme 2 – Schematic representation of a toughened epoxy sample.

3.4.3. X-ray diffraction (XRD)

X-ray diffraction measurements are used to characterize the morphological structure of Cloisite30B/epoxy nanocomposite specimens. It is well known that reflections in the low angle region (0.4–10° 2θ) indicate intercalated nanocomposites. However, the broadening or disappearance of reflections signifies complete exfoliation or disordered intercalates with interlayer space larger than that of the intercalated structure.

In general, the degree of silicate layer dispersion and delamination is usually obtained by X-ray diffraction measurements. Generally, the intense reflections within the range of 1.5–10° (2θ) indicate the formation of an ordered intercalated system with alternating polymer/silicate layers. In the completely delaminated hybrids, silicate layers with a thickness about 1 nm are relatively homogeneously dispersed in the polymer matrix (Dai et al., 2004). Fig. 9 shows the XRD patterns of epoxy/Cloisite-30B nanocomposites and Table 2 shows XRD peak values for neat Cloisite-30B and its epoxy nanocomposites containing 2, 4, 6, 8, and 10 wt% clay contents. Bragg's law has been used to calculate the d-spacing for all specimens (as shown in Eq. (1)).

The characteristic peak (001) of nanoclay appeared at 2θ = 4.62°, therefore the d-spacing of blank nanoclay was determined to be 1.91 nm. The (001) peaks of all wt% of epoxy/Cloisite-30B nanocomposites appeared in the range of 2θ = 2.1°–2θ = 2.3° indicating the presence of intercalations with d-spacing of 4.20 nm–3.83 nm, respectively and almost disappearance of the nanoclay main peak. This is an evidence of complete dispersion of the nanoclay in the epoxy matrix. In addition, by comparing the relative intensities for all nanoclay percentages, it could be concluded that nanoclay dispersion
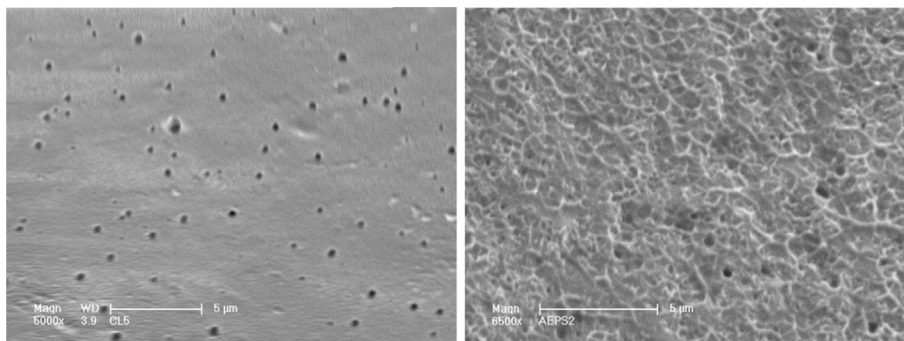
Fig. 7 – SEM micrographs of (left) a simple blend between unfunctionalized rubber nanoparticles and epoxy resin and (right) the reactive blend between epoxidized particles and epoxy resin.
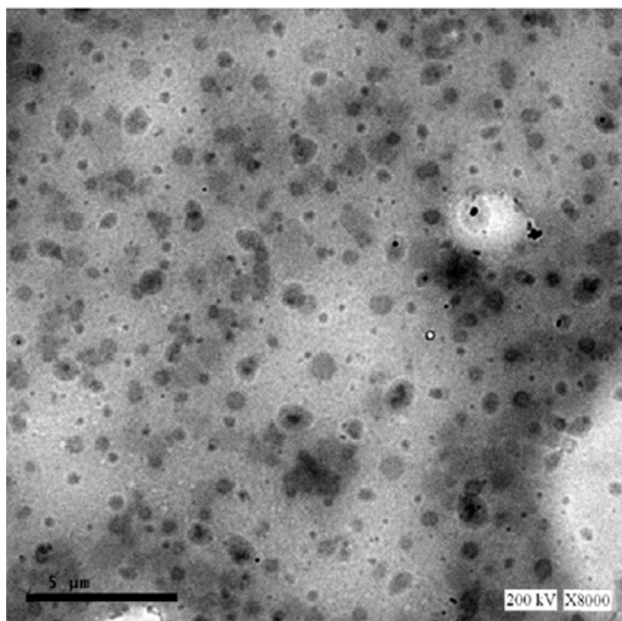

Fig. 8 – TEM micrograph of epoxy toughened with 5% RRNP.

might be in both intercalation and exfoliation modes depending on the nanoclay percentage for each. Based on these d-spacing values and the disappearance of the peak at 4.62 in all nanocomposites; it can be concluded that clay has been completely dispersed into epoxy matrix showing an intercalation mode in all clay percentages. In addition, an important observation could also be noticed by comparing d-spacing for each clay percentage. As the wt% of clay increases from 2 wt% to 10 wt%; there is a noticeable increase in 2θ and consequently an obvious decrease in d-spacing values.

Table 2 – XRD values for Cloisite 30B and its epoxy nanocomposites containing 2, 4, 6, 8, and 10 wt% clay contents.		
Sample (wt%)	$2\theta°$	d-spacing
2	2.10	4.20
4	2.20	4.01
6	2.20	4.01
8	2.23	3.95
10	2.30	3.83
Cloisite 30B	4.62	1.91
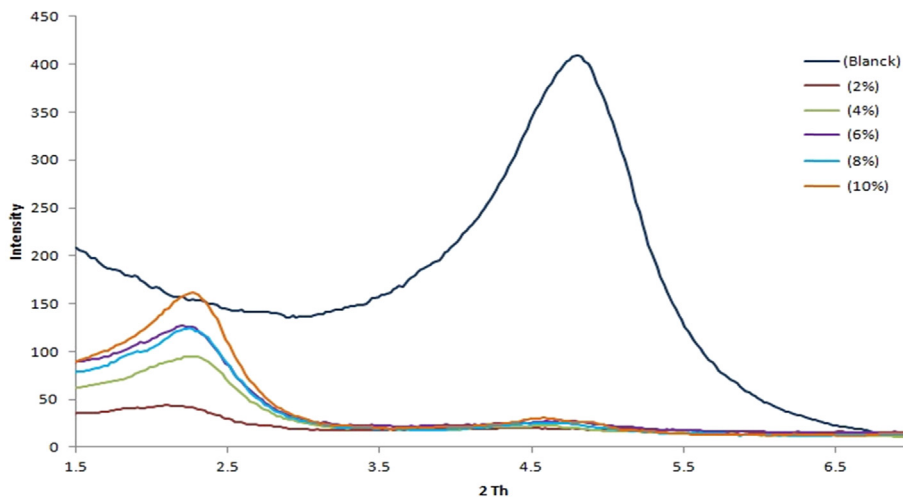
Fig. 9 – X-ray diffraction patterns of Cloisite 30B and epoxy/Cloisite 30B nanocomposites containing 2, 4, 6, 8, and 10 wt% clay contents.

From XRD results; it could be concluded that the inter-gallery spacing of Cloisite-30B facilitates the entry of epoxy or curing agent molecules to enter into the galleries because the hydrophilic clay surface is changed to an organophilic surface. However, completely exfoliated epoxy-clay nano-composites could not be achieved. This is explained by the fact that the extra-gallery curing reaction is faster than the intra-gallery curing reaction. Therefore, no further curing agents or epoxy resins could enter into the galleries and intercalated epoxy-clay nanocomposite is formed (Tak-Keun Oh, 2004). Overall, in order to have a clear visualization of

the nanocomposite microstructure, TEM images of the samples were analyzed.

3.4.4. Transmission electron microscopy (TEM)

In case of epoxy clay nanocomposite, Fig. 10 shows TEM images of 2%, 6% and 10%wt nanoclay epoxy–clay nanocomposite. For 10% wt nanoclay epoxy-clay nanocomposite, both exfoliated clay nanoplatelets (as indicated by green (in the web version) arrows) and intercalated clay nanoplatelets (as indicated by red arrows) were observed with major intercalation mode, while for 2 wt% and 6% wt nanoclay epoxy-clay
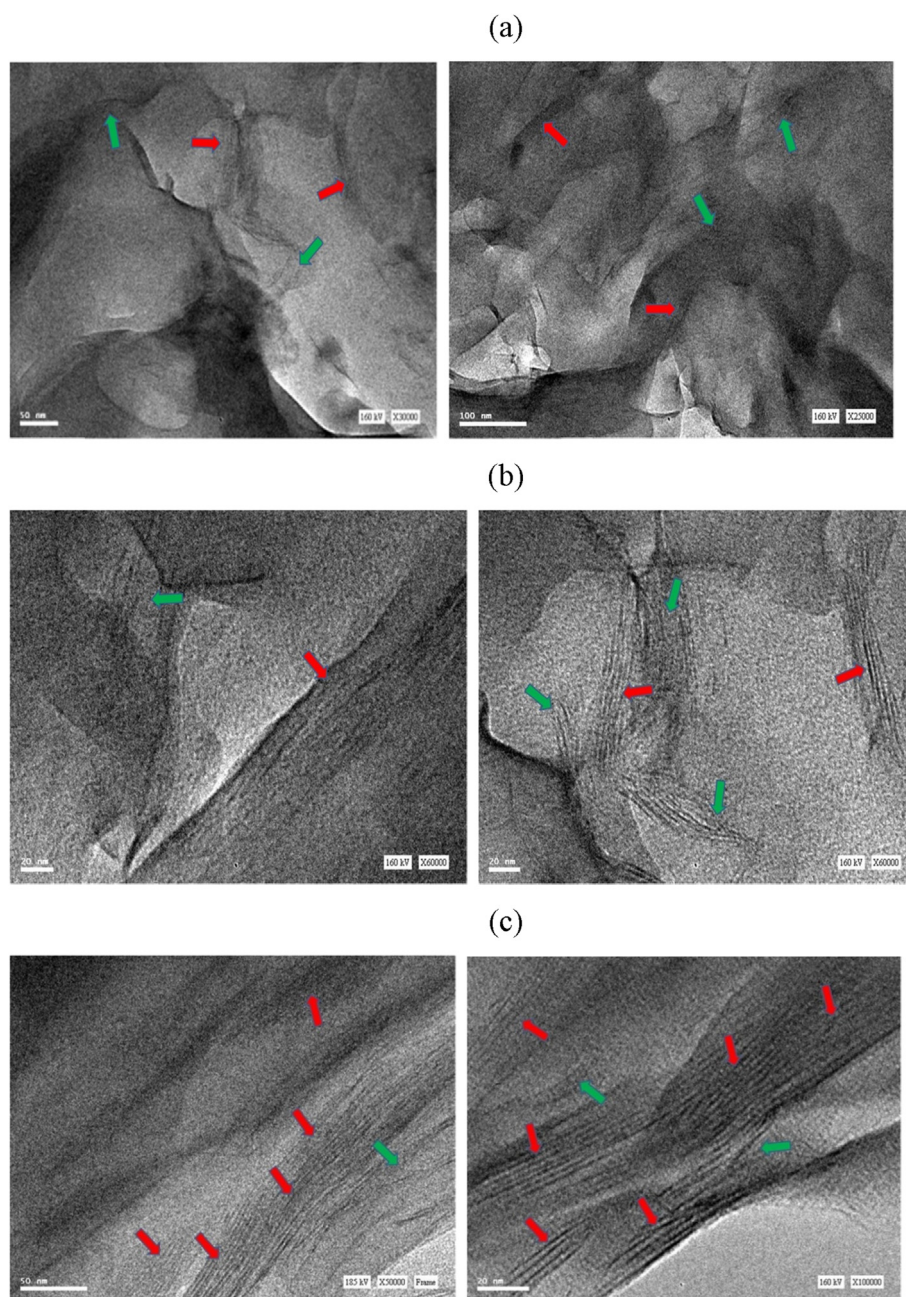
Fig. 10 — TEM images of (a) 2 wt%, (b) 6 wt% and (c) 10 wt% nanoclay epoxy–clay nanocomposite showing exfoliated nanoclay platelets (green arrows) and intercalated nanoclay platelets (red arrows).
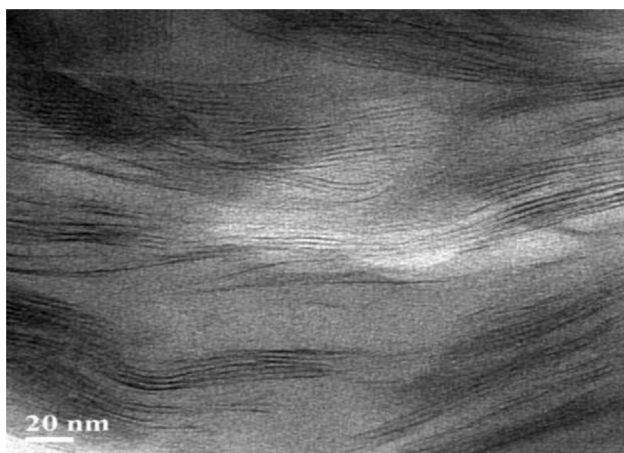
nanocomposite mostly exfoliated clay nanoplatelets (as indicated by green arrows) were observed.

It can be concluded that most of the clay platelets have been dispersed in the exfoliation mode for nanoclay percentage up to 6 wt%. Up to this weight percentage, nanoclay has fully delaminated to silicate layers giving raise to mostly exfoliated nanocomposites with partial intercalated nanoplatelts, which is in consistent with the previous XRD results. On the other hand, increasing the weight percentage of nanoclay in the epoxy matrix resulted in the difficulty of dispersion. This can be noticed from the TEM image of the 10 wt% nanoclay epoxy–clay nanocomposite, where intercalated clay nanoplatelets were observed with some agglomerates.

So, the increased clay mineral loading enhances the ordering of clay mineral layers and gradually degrades the exfoliation potential of the polymer (Chakradhar, Subbaiah, Ashok kumar, & Reddy, 2011). Thus at higher loading, much thicker Cloisite-30B platelets were observed, which confirms the intercalated structure as observed from the XRD results. From these micrographs, again it is clear that the intercalated Cloisite-30B platelets present at 6 wt% loading show enhanced interlayer space compared to 10 wt% loading, thus providing more contact surface area and consequently; better dispersion.

From a combination of X-ray diffraction (XRD) and TEM studies, it can be concluded that the formed epoxy/Cloisite-30B nanocomposites exhibit a mixed morphology that contains well-dispersed (exfoliated) montmorillonite platelets, as well as intercalated tactoids containing multiple montmorillonite layers. These tactoids of parallel-stacked montmorillonite layers (intercalated morphology) gives rise to a definitive d_{001} reflection in wide angle XRD.

In addition, TEM observations indicate similar composite structures for all clay percentage systems, with a slightly better dispersion, more exfoliated single montmorillonite layers and fewer numbers of larger tactoids, with percentage up to 6 wt%. Over this clay loading percentage, most of the dispersed Cloisite-30B is in the intercalated structure.
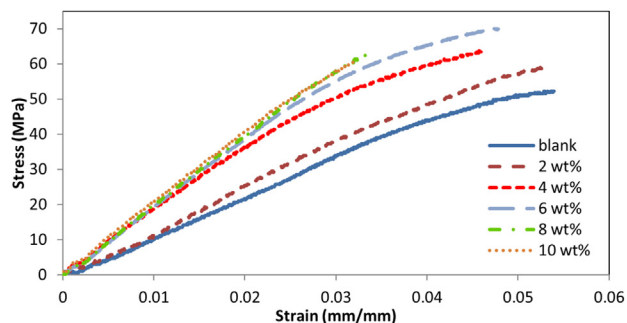
An overall TEM result for a hybrid system composed of both nano-modifiers into the epoxy matrix with optimum percentages is shown in Fig. 11 for a specimen composed of epoxy/6 wt% clay/5 wt% RRNP hybrid.
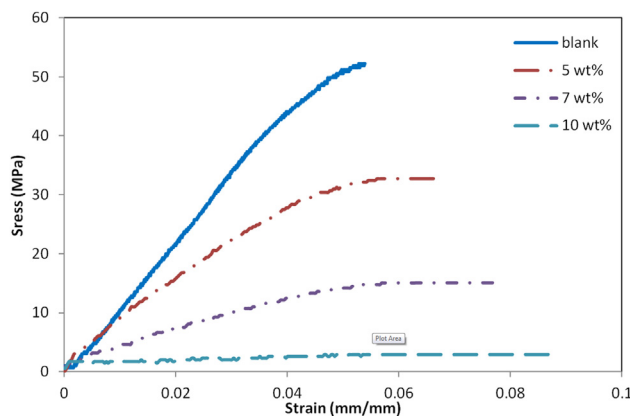
3.5. Mechanical properties

3.5.1. Three point bending flexural test

Flexural stress–strain curves of epoxy/clay, epoxy/RRNP and epoxy/clay/RRNP nanocomposites are given in Figs. 12–14; respectively. It is appeared that the incorporation of nanoclay into epoxy matrix improved its flexural modulus as shown in Fig. 12. The improved modulus can be directly ascribed to the stiffening effect of clay fillers since the clay has a higher modulus than epoxy. The diminishing improvement in flexural modulus at high clay (8%, 10%) contents is attributed to the higher possibility of forming unwanted agglomerates, which in turn reduced the reinforcing efficiency of clay. The improvements of flexural modulus were at the expense of reductions in flexural strength as reported by others (Yasmin, Luo, Abot, & Daniel, 2006; Siddiqui, Woo, Kim, Leung, & Munir, 2007; Isik, Yilmazer, & Bayram, 2003).

Another possible reason for the substantial loss of flexural strength is the presence of internal stresses induced by the different cure rates between the bulk epoxy and the silicate

Fig. 12 — Typical flexural stress–strain curves of pristine resin and nanoclay modified epoxy.

Fig. 11 — High Resolution Transmission Electron Microscopic (HRTEM) images of epoxy/5 wt% RRNP/6 wt% nanoclay nanocomposites.

Fig. 13 — Typical flexural stress–strain curves of pristine resin and RRNP modified epoxy.
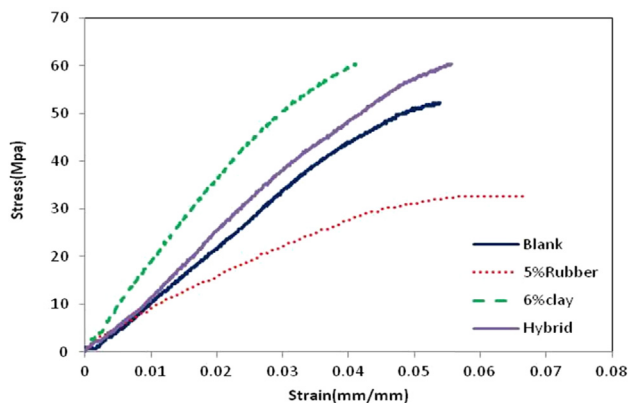
Fig. 14 – Typical flexural stress–strain curves of pristine resin and modified epoxies.

interfaces (Zilg, Thomann, Finter, & Mulhaupt, 2003). In addition, different clay percentages incorporation up-to certain percentage of clay platelets leads to well dispersion (exfoliation) inside the epoxy matrix and consequently this will enhance the interfacial adhesion between the particles and the epoxy matrix (Wei, Zhang, Rong, & Friedrich, 2002). The orientation of clay platelets and polymer chains with respect to the loading direction can also contribute to the reinforcement effects (Liu & Wu, 2001). However, the decreasing rate of flexural modulus improvement with higher clay content can be attributed to the presence of unexfoliated aggregates (Liu & Wu, 2001). This can be observed from Fig. 14 which shows that the optimal clay percentage is 6 wt%.

On another hand, Fig. 13 shows flexural properties of the cured epoxy samples containing different amount of the RRNP. All the modified epoxy networks exhibit higher strain at failure than non-modified epoxy while significantly reducing its stiffness and ultimate strength. The reduction in strength is attributed to the presence of rubber, which is distributed in the epoxy.

Similar findings were reported by other researchers with different types of liquid rubbers (Ratna & Simon, 2001). Based on Fig. 13; it is evident that the best performance was normally achieved with 5 wt% of RRNP which give higher strain than neat epoxy with less stiffness so the higher toughness (area under the curve) than all epoxy/RRNP contents. Similar behavior has been also reported in other rubber-modified epoxy systems and was attributed to the agglomeration of rubber particles with the increase of the rubber concentration (Ratna & Banthia, 2004; Latha, Adhinarayanan, & Ramaswamy, 1994).

Therefore, in the present work; the optimal percentages of nanoclay and RRNP have been incorporated into the epoxy matrix for obtaining the best hybrid flexural properties. Fig. 14 represents typical flexural stress–strain curves of pristine resin and different modified epoxies. All curves show apparent ductility with different modulus, ultimate strength, and fracture strain. The pristine resin has high yield strength but the lowest fracture strain. It is clear from the figure that the incorporation of 5 wt% RRNP into epoxy matrix increases fracture strain. However, this was accompanied by reduction in yield strength, modulus and ultimate strength. On the other hand; the incorporation of 6 wt% nanoclay into epoxy matrix

increases fracture stress with some reduction in the strain value. Consequently; combining these two optimal percentages of RRNP and nanoclay into the epoxy matrix enhanced the flexural stress–strain curve as shown in the formed hybrid.

3.5.2. Dynamic mechanical analysis (DMA)
Generally, DMA determines elastic modulus (or storage modulus, G'), viscous modulus (or loss modulus, G'') and damping coefficient (Tan δ) as a function of temperature, frequency or time. Results are typically provided as a graphical plot of G', G'', and Tan δ versus temperature. This analysis has been applied to provide storage modulus of the obtained nanocomposite specimens. The obtained value is important to evaluate the crosslink length and density. Consequently, these results clear the effect of each nanomaterial on the modified epoxy matrix.

It is known that crosslink density is measured in terms of the number of crosslinks per unit volume or the number average molecular weight between crosslinks, M_c as estimated in Eq. (4).

Where ρ is the density of polymer in (g/cm^3), G_r is the shear equilibrium storage modulus in the rubbery state (Pa), M_c is the crosslink density in g/mol; R and T are real gas constant (8.314 J K^{-1} mol^{-1}) and temperature (in Kelvin), respectively; assuming $q = 1$ at $T = 293$K. Table 3 shows the storage modulus values versus crosslink density (M_c) for clay/epoxy, RRNP/epoxy and clay/RRNP/epoxy nanocomposites at ambient temperature.

Table 3 shows the effect of matrix crosslink density on the dispersion of both fillers inside the epoxy network matrix where storage modulus meanly depends on M_c value. The epoxy resins with lower crosslink density are more ductile; hence the materials endure more plastic shear deformation and dissipate more strain energy (Pearson & Yee, 1989). Comparing storage modulus in case of RRNP with epoxy system; it is clear that due to chemical bond between epoxide groups of RRNP or that of pristine epoxy with the hardener give higher crosslink density leading to a modest reduction in storage modulus than a neat epoxy as shown in Fig. 15.

Therefore, 5 wt% RRNP gave higher cross link density than neat epoxy and consequently toughness increased. Incorporating more RRNP percentages lead to some agglomeration and resulting in decreased of storage modulus.

On the other hand, incorporation of clay increases the stiffness of the epoxy system. Nanoclay is able to act as

| Table 3 – Values of storage modulus (E) vs. crosslink density (M_c) in clay/epoxy, RRNP/epoxy and clay/RRNP/epoxy nanocomposites at ambient temperature.				
Clay (wt%)	Rubber (wt%)	Storage modulus G_r (Pa)	Density (mg/cm^3)	M_c (mg/mole)
0	0	9.05E + 06	0.45	0.124
4	0	1.91E + 07	0.94	0.119
6	0	5.27E + 07	1.11	0.0513
8	0	4.61E + 07	1.38	0.0729
10	0	1.955E + 07	0.91	0.127
0	5	6.47E + 06	0.95	0.357
0	7	4.35E + 06	1.11	0.621
0	10	5.97E + 05	1.22	0.497
6	5	5.97E + 07	0.75	0.306
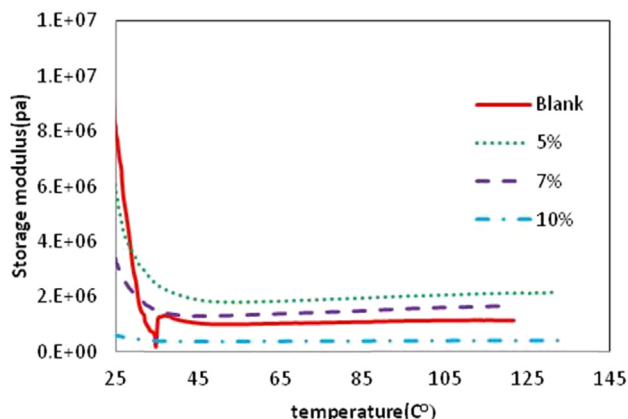
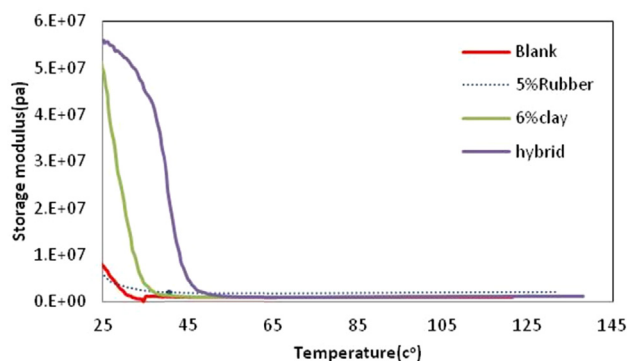Fig. 15 – Storage modulus vs. temperature plots of cured Epoxy/RRNP networks.

reinforcing filler owing to its high aspect ratio and platelet structure, but the intercalation and exfoliation of clay platelets in epoxy serve to effectively decrease in crosslink density as shown in Table 3. That is mean as the number of exfoliated platelets increased as the crosslink density decreased due to molecular mobility. Therefore, sample of 6 wt% of nanoclay containing higher amount of exfoliated platelets has the lowest crosslink density which is in consistent with XRD and TEM results.

The well dispersed nanoclay in epoxy becomes more effective in retarding matrix molecular mobility, thus increasing the storage moduli as shown in Fig. 16. Similar observations were reported in the literature with various epoxy matrices (Ratna, Manoj, Varley, Raman Singh, & Simon, 2003). It can be seen that the storage modulus increases with increasing clay content up to 6 wt% at rubbery region. Further increase in clay loading decreases the modulus. The improvement in modulus can be directly ascribed to the stiffening effect of clay fillers since the clay has a higher modulus than epoxy. It has been already reported in many epoxy/clay nanocomposites that the increments in modulus of the clay filled epoxy system were subjected to the "rule of mixtures" (Nielsen & Landel, 1994).

Fig. 17 shows the storage moduli of the hybrid nanocomposites as a function of temperature. The storage modulus was found to decrease with the addition of 5 wt%
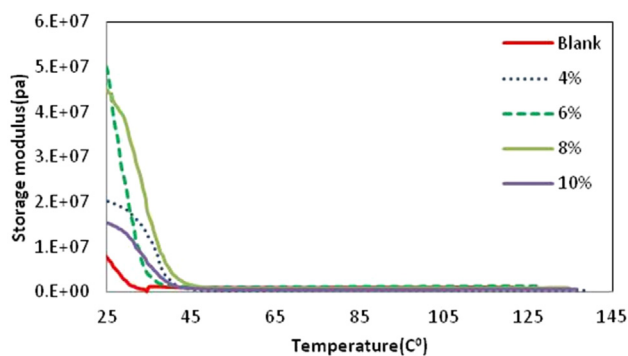
Fig. 16 – Storage modulus vs. temperature plots of cured epoxy/nanoclay networks.

Fig. 17 – Storage modulus vs. temperature plots of epoxy/RRNP, epoxy/nanoclay and epoxy/RRNP/nanoclay hybrid composites.

RRNP as expected, since the presence of the soft rubbery particles will reduce the stiffness of the relatively rigid epoxy polymer. Whereas incorporation of 6 wt% nanoclay results in significant increase in storage modulus.

Hence the resultant modulus of epoxy/RRNP/nanoclay nanocomposite is significantly higher compared to the neat epoxy. The storage modulus of hybrid nanocomposite is about five times higher than that of unfilled epoxy. This is a strong advantage of addition both additive nanoparticles over the neat polymer.

4. Conclusion

In this work, epoxy/clay/RRNP nanocomposites have been successfully prepared by *in situ* polymerization. Mechanical testing, X-ray diffraction (XRD), Fourier transform infrared spectroscopy (FTIR) and transmission electron microscopy (TEM) were used to measure mechanical, microstructure and morphological properties of the hybrid nanocomposites. Hybrid composites containing (o-mmt) or (RRNP) or both comprise intercalated nanoclay embedded in a homogeneous epoxy matrix. Incorporation of RRNP results in a softened nanocomposite with lower stiffness and improved toughness compared to those of the neat resin. In contrast, incorporation of (o-mmt) in the cured epoxy increased the stiffness and lowered the toughness of the epoxy/nanocomposites compared to those of the neat resin. The morphology of the nanocomposites consists of both exfoliated and intercalated clay structures as evidenced by X-ray diffraction (XRD) and transmission electron microscopy (TEM). The present study is an extended work to characterize the mechanical properties of epoxy and its organoclay nanocomposites, including storage modulus curve by using dynamic mechanical analyzer technique (DMA) and the observed changes are rationalized in the three points bending flexural test data.

REFERENCES

ASTM D 790-03. (2008). *Flexural properties of unreinforced and reinforced plastics and electrical insulating materials, annual book of ASTM standards*. Philadelphia, PA.

Bashar, M., Sundararaj, U., & Mertiny, P. (2011). Study of matrix micro-cracking in nano clay and acrylic tri-block-copolymer modified epoxy/basalt fiber-reinforced pressure-retaining structures. *Express Polymer Letters, 5*(10), 882–896.

Becher, P. (1965). *Emulsions: Theory and practice, ACS monograph series no. 162* (2nd ed.).

Chakradhar, K. V. P., Subbaiah, K. V., Ashok kumar, M., & Reddy, G. R. (2011). Epoxy/polyester blend nanocomposites: effect of nanoclay on mechanical, thermal and morphological properties. *Journal of Malaysian Polymer, 6*, 109–118.

Crivello, J. V., & Song, S. (2000). Synthesis and cationic photo polymerization of novel monomers based on dicyclopentadiene. *Chemistry of Materials, 12*, 3674–3680.

Dai, X., Xu, J., Guo, X., Lu, Y., Shen, D., Zhao, N., et al. (2004). Study on structure and orientation action of polyurethane nanocomposites. *Macromolecules, 37*, 5615–5623.

Ferry, J. D. (1980). *.Viscoelastic properties of polymers* (3rd ed.). New York: Wiley.

Giannelis, E. P. (1996). Polymer layered silicate nanocomposites. *Advanced Materials, 8*, 29–35.

Harani, H., Fallahi, S., & Bakar, M. (1998). Toughening of epoxy resin using synthesized polyurethane prepolymer based on hydroxyl-terminated polyesters. *Applied Polymer Science, 70*, 2603.

Hsieh, T. H., Kinloch, A. J., Masania, K., & Taylor, A. C. (2010). The mechanisms and mechanics of the toughening of epoxy polymers modified with silica nanoparticles. *Polymer, 51*, 6284–6294.

Isik, Yilmazer, U., & Bayram, G. (2003). Impact modified epoxy/montmorillonite nanocomposites: synthesis and characterization. *Polymer, 44*(20), 6371–6377.

Kandil, U. F. (2005). Dissertation titled: novel functional ethylene/propylene elastomers: synthesis and characterization. *Material Science Engineering*. phd dissertation, Chapter 2, 60-65.

Kim, I. (2001). Copolymerization of ethylene and 5-vinyl-2-norbornene by stereospecific metallocenes and epoxidation of the resulting copolymer. *Reactive Functional Polymers, 49*, 197–204.

Kojima, Y., Usuki, A., Kawasumi, M., Okada, A., Fukushima, Y., Kurauchi, T., et al. (1993). Mechanical properties of nylon 6-clay hybrid. *Journal of Materials Research, 8*, 1185–1189.

Latha, P. B., Adhinarayanan, K., & Ramaswamy, R. (1994). Epoxidized hydroxy-terminated polybutadiene – synthesis, characterization and toughening studies. *International Journal of Adhesion and Adhesives, 14*(1), 57–61.

Lee, J., & Yee, A. F. (2000). Role of inherent matrix toughness on fracture of glass bead filled epoxies. *Polymer, 41*, 8375–8385.

Liu, X., & Wu, Q. (2001). PP/clay nanocomposites prepared by grafting-melt intercalation. *Polymer, 42*(25), 10013–10019.

Messersmith, P. B., & Giannelis, E. P. (1994). Synthesis and characterization of layered silicate-epoxy nanocomposites. *Chemistry of Materials, 6*, 1719–1725.

Michael, F., DiBerardino, & Raymond, A. (2009). The effect of particle size on synergistic toughening of boron nitride-rubber hybrid epoxy composites. *Toughening Plastics, 759*, 213–229.

Mülhaupt, R. (1994). *Phenol-terminated polyurethane or polyurea (urethane) with epoxy resin*. US 5278257.

Nielsen, L. E., & Landel, R. F. (1994). *Ch. 7 in mechanical properties of polymers and composites* (2nd ed.). New York: Marcel Dekker.

Tak-Keun Oh. (2004). *The effect of shear force on microstructure and mechanical property of epoxy/clay nanocomposite*. Master of Science; University of Florida.

Ohama, Y. (1995). *Handbook of polymer-modified concrete and mortars: Properties and process technology*. USA: William Andrew.

Pascault, J.-P. (1995). Rubber and thermoplastic-modified polymer networks. Phase separation process induced by polymerization and polycondensation. *Macromolecular Symposia, 93*, 43–51.

Pearson, R. A., & Yee, A. F. (1989). Toughening mechanisms in elastomer-modified epoxies. *Journal of Materials and Science, 24*, 2571–2580.

Rajabi, F. H., Alavi Nikje, M. M., & Taslimipour, T. (2010). Epoxidation of styrene–butadiene rubber (SBR) using in situ generated dimethyldioxirane (DMD): characterization and kinetic study. *Designed Monomers and Polymers, 13*, 535–546.

Ratna, D., & Banthia, A. K. (2004). Rubber toughened epoxy. *Journal of Applied Polymer and Science, 12*, 11–21.

Ratna, D., Manoj, N. R., Varley, R., Raman Singh, R. K., & Simon, G. P. (2003). Clay-Reinforced epoxy nanocomposites. *Polymer International, 52*, 1403–1407.

Ratna, D., & Simon, G. P. (2001). Mechanical characterization and morphology of carboxyl randomized poly (2-ethyl hexyl acrylate) liquid rubber toughened epoxy resins. *Polymer, 42*, 7739–7747.

Sharmin, E., Akram, D., Ghosal, A., Rahman, O., Zafar, F., & Ahmad, S. (2011). Preparation and characterization of nanostructured biohybrid. *Progress in Organic Coatings, 72*, 469–472.

Siddiqui, N. A., Woo, R. S. C., Kim, J. K., Leung, C. C. K., & Munir, A. (2007). Mode I interlaminar fracture behavior and mechanical properties of CFRPs with nanoclay-filled epoxy matrix. *Composites Part A, 38*, 449–460.

Wei, C. L., Zhang, M. Q., Rong, M. Z., & Friedrich, K. (2002). Tensile performance improvement of low nanoparticles filled-polypropylene composites. *Composites Science and Technology, 62*, 1327–1340.

Yasmin, A., Luo, J. J., Abot, J. L., & Daniel, I. M. (2006). Mechanical and thermal behavior of clay/epoxy nanocomposites. *Composites Science and Technology, 66*(14), 2415–2422.

Yi, I., Wiedmaier, J., & Schmauder, S. (2015). Modeling and simulation of mechanical properties of nano particle modified polyamide 6. *Journal of Materials Science and Chemical Engineering, 3*(1).

Zilg, C., Thomann, R., Finter, J., & Mulhaupt, R. (2000). The influence of silicate modification and compatibilizers on mechanical properties and morphology of anhydride–cured epoxy nanocomposites. *Macromolecular Materials and Engineering, 41*, 280–281.